Journal of Inorganic and General Chemistry
ZAAC
Zeitschrift für anorganische und allgemeine Chemie
www.zaac.wiley-vch.de
RESEARCH ARTICLE
Check for updates
DOI: 10.1002/zaac.202400180

Rare-Earth 4-Hydroxyphenylacetate Complexes: Synthesis, Structural Characterization, and Corrosion Inhibition Properties

Naveena Yasaswin Salpadoru Thuppahige, Zhifang Guo, Glen B. Deacon, Anthony E. Somers, and Peter C. Junk*

This paper is dedication to Professor Dr Hubert Schmidbauer (TU München) on the occasion of his 90th birthday and for his stellar contributions to Inorganic Chemistry

Four structural types of rare-earth aqua 4-hydroxyphenylacetate complexes $\{[Ce(L)_3(H_2O)_2]\cdot H_2O\}_n$ (**a**), $\{[RE_2(L)_6(H_2O)]\cdot 4H_2O]\}_n$ (RE = Nd (**b**), Gd (**c**)), $\{[RE_2(L)_6(H_2O)]\cdot 3H_2O]\}_n$ (RE = Dy (**d**), Y (**e**)), $\{[RE_2(L)_6(H_2O)]\cdot 5H_2O]\}_n$ (RE = Er (**f**), Yb (**g**)), (L = 4-hydroxyphenylacetate) have been synthesized by salt metathesis reactions of corresponding rare-earth metal chlorides or nitrates and sodium 4-hydroxyphenylacetate (NaL) in a water/ethanol solvent system. The compounds are targeted for structural interest and to determine if the 4-hydroxy (4-OH) substituent would enhance the anti-corrosion properties of rare-earth phenylacetates. Single crystal X-ray diffraction (XRD) determined the crystal structures of all compounds except the complex of Gd (**c**), which was shown to be isomorphous with the Nd complex (**b**) by the powder XRD pattern. All compounds were obtained as one-dimensional polymeric structures. The structure of **a** differs in being a monometallic repeating unit and having two coordinated waters whilst the others have binuclear repeating units that resulted from the alternating coordination of one water molecule along the chain. Weight loss and potentiodynamic polarization tests reveal that $\{[Gd_2(L)_6(H_2O)]\cdot 4H_2O\}_n$ has the best corrosion inhibition properties for mild steel in 0.01 M NaCl. Furthermore, all **a**–**g** complexes are more effective corrosion inhibitors than the aqua and 2,2′-bipyridine (bpy) complexes of unsubstituted phenylacetate indicating that 4-OH substitution of phenylacetate enhances anti-corrosion properties.

1. Introduction

The process of corrosion involves the degradation of metals and alloys, resulting in functional or structural deterioration or failures of their roles due to loss of mechanical or other properties.[1,2] This phenomenon impacts numerous sectors such as construction, manufacturing, automobiles, chemical plants, cooling towers, radiators, and medical applications.[3,4] As a result, in the modern world, corrosion has become a crucial issue, and it is estimated that the global cost of corrosion for new constructions, reparation, and maintenance expenses was US$2.5 trillion per year in 2013.[2,5] To reduce the damage and save huge amounts of time and money, several measures including structure design, alloying, coating, cathodic and anodic protection, alteration of the system environment, addition of corrosion inhibitors and laser technology have been utilized over time.[1,6] To overcome this natural phenomenon, corrosion inhibitors play a significant role as an effective, simple, and comparatively economical solution.[7,8] The addition of a small amount of the inhibitor to the corrosive environment, can significantly reduce the rate of the corrosion process.[9]

Chromium (VI) salts have been exceptional corrosion inhibitors for many metals and alloys for over a century, acting as both anodic and cathodic inhibitors.[10,11] Nevertheless, the extreme toxicity for humans and the environmentally hazardous nature of these compounds have led to imposing legal restrictions on their usage.[12] Additionally, molybdate, phosphate, and tetraborate have been reported as efficient corrosion inhibitors.[13] Amongst these inorganic inhibitors including chromium salts, rare-earth (RE) metal salts such as Ce(III), Pr(III), and La(III) were investigated as efficient, less toxic, and eco-friendly corrosion inhibitors in the mid-1980s.[3,14–16] In the studies by Hinton et al. it has been found that RE metal salts function as cathodic inhibitors.[15,16] Moreover, organic compounds have also been found to perform as effective corrosion inhibitors in various environments, especially even in an acidic medium.[17,18] They achieve this corrosion inhibition ability because of their specific molecular structure, which consists of heteroatoms, lone pairs, polar functional groups, conjugated double, or triple bonds aiding interaction with the metal surface.[4,5,19–21] However, the inherent properties like poor solubility in polar solvents and thermal

N. Y. Salpadoru Thuppahige, Z. Guo, P. C. Junk
College of Science & Engineering, James Cook University, Townsville, QLD 4811, Australia
E-mail: peter.junk@jcu.edu.au
G. B. Deacon
School of Chemistry, Monash University, Clayton, VIC 3800, Australia
A. E. Somers
Institute for Frontier Materials, Deakin University, Burwood, VIC 3125, Australia

Supporting information for this article is available on the WWW under https://doi.org/10.1002/zaac.202400180

instability limit their usage in many cases.[17,22] Among organic inhibitors, carboxylates at higher concentrations are effective with mainly anodic inhibition.[11]

Forsyth et al. combined RE metals and aromatic carboxylates giving complexes that can exhibit both cathodic and anodic protection processes. As the first step, they discovered that cerium salicylate shows synergetic corrosion resistance compared to individual performances of Ce^{III} salts and sodium salicylate.[23,24] Later, this concept was extended to cinnamate compounds of cerium and lanthanum cations, particularly lanthanum complexes of 4-hydroxycinnamate and 4-nitrocinnamate, which functioned as excellent inhibitors, comparable to sodium chromate ($Na_2Cr_2O_7$) even at very low concentrations.[25,26] In the last 20 years, various novel RE carboxylates have been discovered as corrosion inhibitors for steel[27] and well-performing RE metal carboxylates such as 3-(4′-hydroxyphenyl)-propionate,[28] 3-thiophenecarboxylate,[29] and 2-methyl-3-furoate[30] were reported. Among them, some compounds including yttrium aqua complexes of 4-hydroxybenzoate,[31] yttrium 3-(4′-methylbenzoyl)-propanoate,[11] and yttrium 3-furoate[32] outperformed earlier best corrosion inhibitors. One of our recent studies focused on RE-phenylacetate[33] compounds to study the performance of a simple carboxylate and probe the necessity of extra functional groups beyond the carboxylate for good corrosion inhibition properties. These compounds exhibited poor inhibition efficacy,[33] indicating the need for additional functionality.

Given that the 4-hydroxy substituent in the phenyl ring of cinnamate greatly enhances anti-corrosion performance,[25] it was of interest to see if a 4-hydroxy substituent could have a similar advantageous effect on phenylacetate. Moreover, in the recent study on La, Ce, and Y 4-hydroxybenzoate (4hob) complexes as corrosion inhibitors for mild steel, the inhibition performances of the 4hob complexes were much better than that of the established inhibitor, cerium salicylate.[31] Again a 4-OH substituent induced improved performance. Thus, the corrosion inhibition performance of RE 4-hydroxyphenylacetate complexes (**Figure 1** for 4-hydroxyphenylacetate L^-) has been examined with the RE metals selected representing the different ionic radii of RE cations. Initially, the synthesis and structures of RE aqua 4-hydroxyphenylacetate complexes had to be investigated.

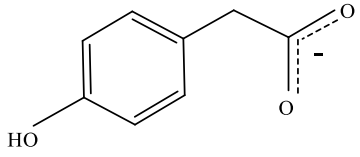

Figure 1. Structure of 4-hydrophenylacetate (L^-).

4-hydroxyphenylacetate is a derivative of the popular phenylacetate ligand that has the potential to provide metal complexes with unique properties.[34] A lanthanum 4-hydroxyphenylacetate has been prepared for use in explosive detection and as a source of La nanoparticles.[35] The hydroxyl group in the 4-hydroxyphenylacetate contributes to molecular stability by forming hydrogen-bonding interactions.[35] The more highly substituted 2,5-dihydroxy-1,4-dicarboxylate has been widely employed to provide a range of structural topologies with SMM and magnetocaloric properties.[36–39] Accordingly, these ligands have wider application than their use in corrosion inhibitors.

2. Results and Discussion

2.1. Synthesis and Characterization

The complexes of selected rare-earth (RE) metals (Ce, Nd, Gd, Dy, Y, Er, and Yb) were synthesized by salt metathesis reactions between sodium 4-hydroxyphenylacetate and the RE salt (mole ratio 3:1), as shown in **Scheme 1**.

After the reaction, only the complexes of Ce, and Nd were precipitated (bulk sample) while the other metal complexes remained soluble. Single crystals of all the complexes were obtained by slow evaporation of the mother liquor and they were used for X-ray crystallography except for the Gd complex. The crystal size and quality of the Gd compound were inadequate for single- crystal XRD determination but was isomorphous with the Nd analog by XRPD. The XRPD of the freshly isolated Er complex showed it to be isomorphous with the Yb analog (**Figure 2**iv), but microanalysis after transport to London showed loss of two of the water molecules of crystallization, and this was confirmed by TGA on a similar sample. In all cases, the XRPD of the bulk sample was in agreement with the pattern simulated from the crystal structure (Figure 2) and the composition of the products (Scheme 1) from elemental analysis was in agreement with the single-crystal composition except for the Er complex.

TGA of the six complexes **b**–**g** indicates a single weight loss, in the range 25–150 °C, which is associated with the loss of both lattice water and coordinated water molecules consistent with their crystal composition (Figure S2, Supporting Information), except for the Er complex **f** discussed above. The TG curve of

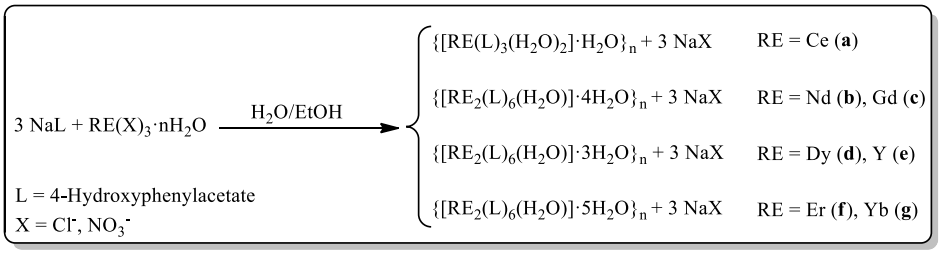

Scheme 1. Synthesis of RE 4-hydroxyphenyacetate complexes **a**–**g** by metathesis reactions.

Journal of Inorganic and General Chemistry
ZAAC
Zeitschrift für anorganische und allgemeine Chemie

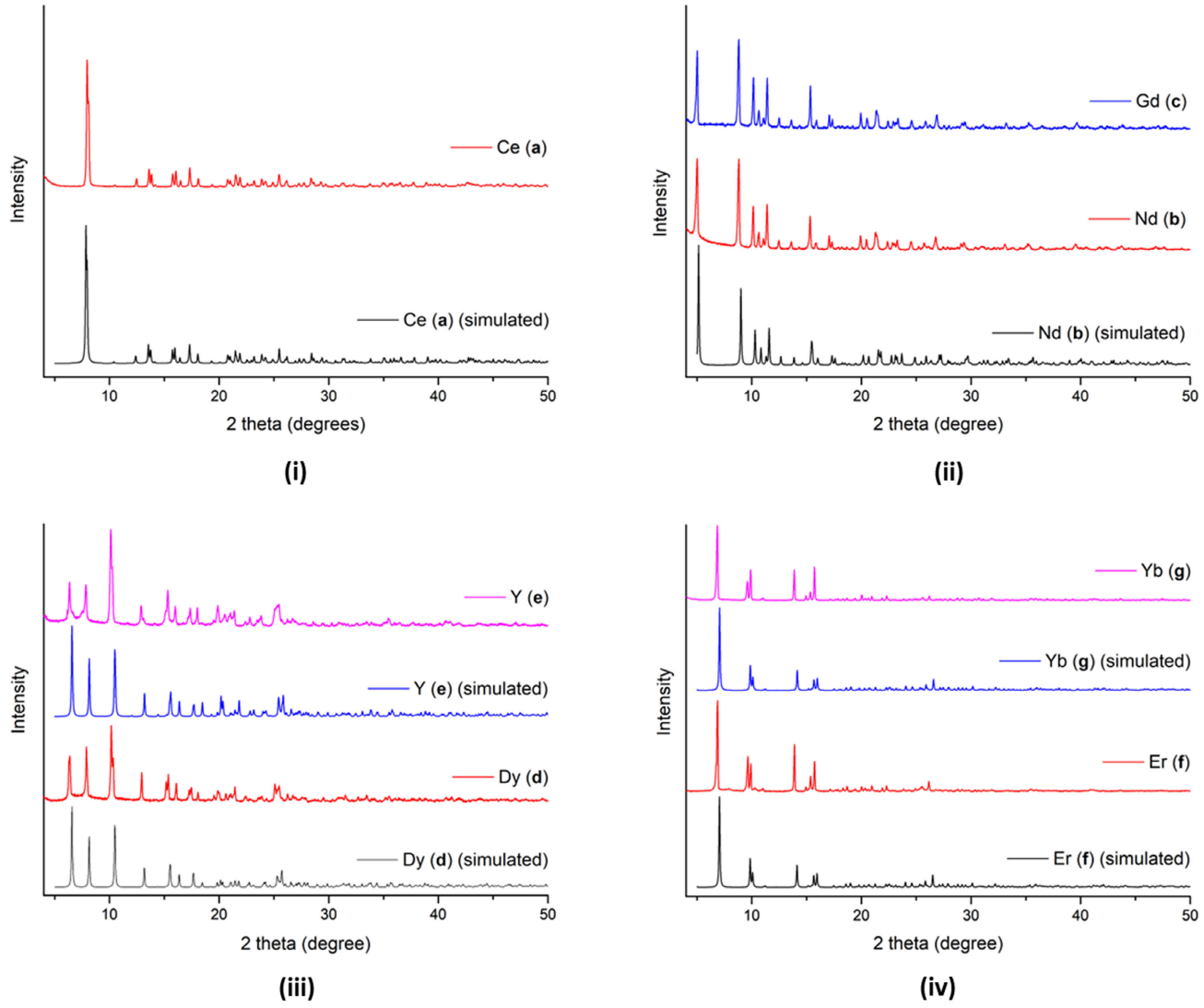

Figure 2. PXRD traces ($2\theta = 4°–50°$) of i) Complex $\{[Ce(L)_3(H_2O)_2]\cdot H_2O\}_n$ **a**; ii) Complexes $\{[RE_2(L)_6(H_2O)]\cdot 4H_2O\}_n$ (RE = Nd **b**, Gd **c**); iii) Complexes $\{[RE_2(L)_6(H_2O)]\cdot 3H_2O\}_n$ (RE = Dy **d**, Y **e**); iv) Complexes $\{[RE_2(L)_6(H_2O)]\cdot 5H_2O\}_n$ (RE = Er **f**, Yb **g**) compared to their simulated patterns.

$\{[Ce(L)_3(H_2O)_2]\cdot H_2O\}$ (Figure S1, Supporting Information) resulted in a total weight loss of 8.2% in two steps; 1) weight loss of 5.6% attributed to loss of water of crystallization and one coordinated water molecule 2) weight loss of 2.6% corresponding to the remaining coordinated water. Further weight loss of ≈16% around 200–400 °C for compounds **a**–**f** and around 200–270 °C for compound **g** was observed, sometimes in two steps (Figure S1 and S2, Supporting Information). The percentage weight loss for all compounds except **a** and **e** is consistent with the removal of $(4\text{-}HOC_6H_4CH_2)_2$ (R_2) (Table S12, Supporting Information). Partial decarboxylation gives a coordinated oxalate ion and a dialkyl molecule from the formation and dimerization of R′ radicals (Equation (1)). Continuation of the weight loss immediately following this stage indicates further decomposition occurs which may finish with RE oxide or carbonate.[32] For **a** and **e**, a better fit can be obtained by decomposition into $RE_2(O_2CR)_4(CO_3)$ and the ketone R_2CO (Table S12, Supporting Information), but is not satisfactory for the other five complexes.

$$2\,RE(O_2CR)_3 \rightarrow RE_2(O_2CR)_4(C_2O_4) + R_2 \quad (1)$$

In the IR spectra, several specific peaks corresponding to the functional groups of the complexes could be identified (**Table 1**; Figure S4, Supporting Information). The spectra of iso-structural complexes show close similarity. A strong peak at 1701 cm^{-1} which corresponds to carbonyl (C=O) stretching was observed in the spectrum of free 4-hydroxyphenyl acetic acid (Figure S3, Supporting Information). The absence of this absorption in all compounds' spectra verifies the deprotonation of the carboxylic acid group and coordination of the COO^- group.[40] For all the complexes, the broad band within the range 3500–3100 cm^{-1} is attributed to the OH stretching vibrations of water molecules and the hydroxyl group of the 4-hydroxyphenylacetate ligand.[41] IR spectra of all compounds exhibit asymmetric and symmetric stretching bands at 1546–1513 and 1397–1405 cm^{-1}, respectively. Furthermore, the values of Δν (the difference between asymmetric and symmetric vibrations) are less than that (146.5 cm^{-1}) of the sodium

Table 1. Selected infrared bands (cm^{-1}) of the RE 4-hydroxyphenylacetate complexes.

Compound	ν(OH)water	$\nu_{as}(COO^-)$	$\nu_s(COO^-)$	$\Delta\nu = (\nu_{as}-\nu_s)avg$
LH	3234	1560, 1546, 1516	1405	136
NaL		1546, 1509	1381	147
$\{[Ce(L)_3(H_2O)_2]\cdot H_2O\}_n$ (**a**)	3267	1546, 1513	1404	126
$\{[Nd_2(L)_6(H_2O)]\cdot 4H_2O\}_n$ (**b**)	3271	1542, 1515	1397	132
$\{[Gd_2(L)_6(H_2O)]\cdot 4H_2O\}_n$ (**c**)	3304	1542, 1516	1401	128
$\{[Dy_2(L)_6(H_2O)]\cdot 3H_2O\}_n$ (**d**)	3333	1530, 1514	1405	117
$\{[Y_2(L)_6(H_2O)]\cdot 3H_2O\}_n$ (**e**)	3276	1530, 1514	1405	117
$\{[Er_2(L)_6(H_2O)]\cdot 5H_2O\}_n$ (**f**)	3327	1528, 1514	1405	116
$\{[Yb_2(L)_6(H_2O)]\cdot 5H_2O\}_n$ (**g**)	3327	1534, 1514	1400	124

carboxylate. This suggests the presence of bridging and/or chelating carboxylate groups, and the absence of monodentate ligands.[42,43]

2.2. Structural Description

All structures in this study have only three types of carboxylate binding as shown in **Figure 3**. The experimental crystallographic data and refinement details are given in Table S1, Supporting Information.

2.2.1. The Complex $\{[Ce(L)_3(H_2O)_2]\cdot H_2O\}_n$

The asymmetric unit of the Ce complex (**a**) consists of one Ce(III) ion, which is coordinated by three 4-hydroxyphenylacetate (L) ligands and two water molecules, and with one uncoordinated water molecule in the lattice. The compound crystallized in the monoclinic crystal system and $P2_1/c$ space group. Part of the structure (**Figure 4**) shows the repeating unit of the polymeric array.

One Ce ion is surrounded by five carboxylate ligands and two water molecules. Among the five carboxylates, four exhibit a chelating bridging binding mode and are tridentate, whereas the other is *syn-syn* asymmetric (0.12 Å difference) chelating (O1,2). Two of these chelating bridging carboxylates bind to Ce1 through both of their O atoms of (O4,5), and (O7*,8*), while the other two bind to the same Ce1 metal ion through one O atom (O5#, and O7). Additionally, the metal ion is coordinated by two *cisoid* water molecules (O10-Ce1-O11 67.793(5)). Thus, the coordination number of Ce1 is 10 having bicapped square antiprismatic stereochemistry. The structure is a 1D polymeric chain through

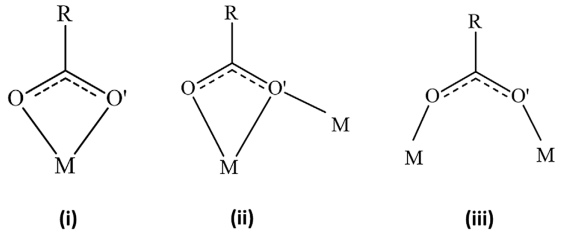

Figure 3. Coordination modes of 4-hydroxyphenylacetate in **a**–**g**: i) *syn-syn* chelate - κ(O,O′); ii) chelating bridging - Z,E-μ-1κ(O)-2κ(O,O′); iii) *syn-syn* bridging – Z,Z-μ-1κ(O)-2κ(O′).

two chelating bridging carboxylate ligands. The distances between adjacent Ce1-Ce1* and Ce1-Ce1# metal ions are 4.3863(4), and 4.5310(4) Å respectively, with an angle of 147.786(4) at Ce1 (Ce1*-Ce1-Ce1#). The angles between Ce1 and Ce1# at both bridging oxygen atoms O5 and O5# (Ce1-O5/O5#-Ce1#) are 119.279(5)° and the angle Ce1-O7/ O7*-Ce1* is 115.135(6)°. The Ce complex is isomorphous with the recently reported La analog.[35]

The average bond length between Ce1 and the carboxylate oxygen (Ce1-O) is 2.598 Å, which is somewhat longer than <Ce-OH2> (2.527 Å). The difference between <Ln-O> for Ce-O and the 10 coordinate Nd1-O (**Table 2**) is as expected for the ionic radius difference.[44]

2.2.2. The Complexes $\{[RE_2(L)_6(H_2O)]\cdot 4H_2O]\}_n$ (RE = Nd, Gd)

The isomorphous complexes (**b**) and (**c**) form a 1D polymeric structure and crystallize in the monoclinic C2/c space group. The representative structure of $\{[Nd_2(L)_6(H_2O)]\cdot 4H_2O]\}_n$ (asymmetric unit and a part of the polymeric chain) is shown in **Figure 5**. The asymmetric unit has two different Nd^{III} ions, three carboxylate molecules, and one water ligand. In addition, two uncoordinated water molecules are present (O11, and O12).

All carboxylate ions exhibit the chelating bridging binding mode (ii). The Nd1 ion is surrounded by 10 oxygen atoms (O1, O2, O4, O5, O7, O1*, O2*, O4*, O5*, and O7*) from six chelating binding carboxylates and has bicapped square antiprismatic stereochemistry. Of these six chelating bridging carboxylate ligands, four bind as bidentate to Nd1 (O1, O2), (O4, O5), (O1*, O2*), (O4*, O5*) and the other two are monodentate (O7, and O7*) to Nd1. The coordination sphere around the Nd2 ion consists of four chelating oxygen atoms (O7, O8), (O7$, O8$) from two chelating bridging carboxylates, four bridging oxygens (O2, O5, O2$, O5$) from four such carboxylates, and one coordinated water molecule (O10). Nd2 is nine coordinate and the geometry about the metal is tricapped trigonal prismatic.

All Nd metal ions are bridged by carboxylates to create a one-dimensional polymeric chain with a Nd….Nd distance of 3.9747(4) Å between adjacent Nd1 and Nd2. Three chelating bridging carboxylates (through O2, O5, O7) link the two metal ions along the chain. The angles Nd1–Nd2–Nd1# and Nd2–Nd1–Nd2* (122.063(10°), and 180°, respectively) differ

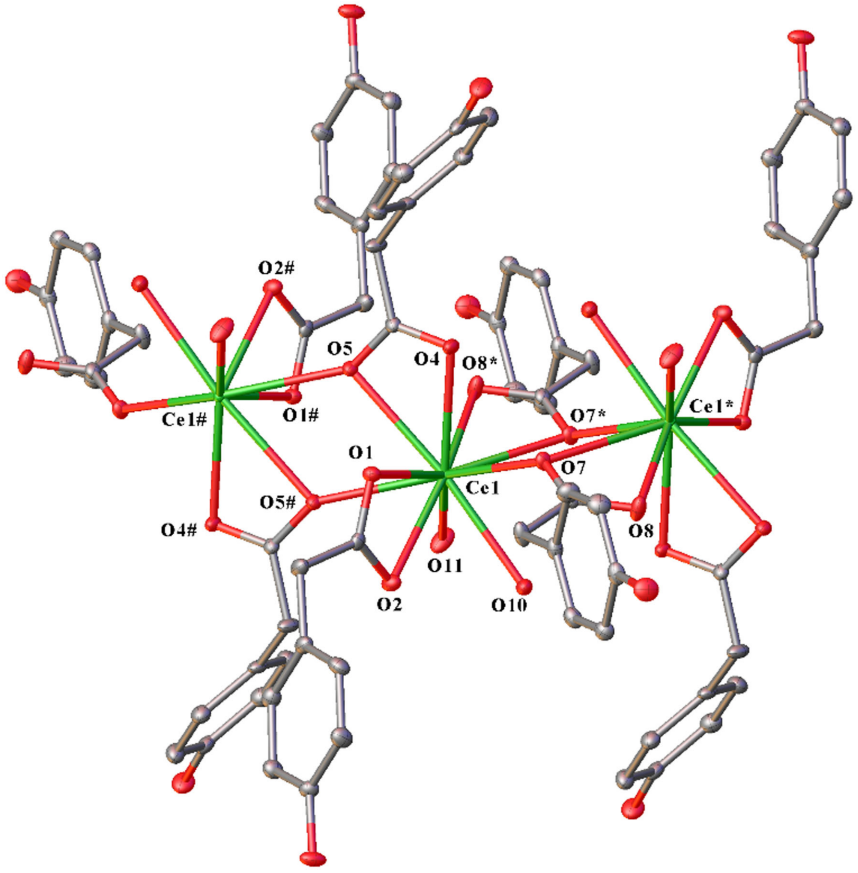

Figure 4. A part of the polymeric chain of $\{[Ce(L)_3(H_2O)_2]\cdot H_2O\}_n$ **a** with 50% thermal ellipsoids. Hydrogen atoms have been omitted for clarity. Symmetry Code: #2 − X, 1 − Y, 1 − Z; *1 − X, 1 − Y, 1 − Z.

Table 2. Average RE-O (carboxylate) bond lengths in RE 4-hydroxyphenylacetate complexes. (CN = coordination number).

RE 4-hydroxyphenylacetate complex	RE1		RE2	
	CN	RE1-O [Å]	CN	RE2-O [Å]
$\{[Ce(L)_3(H_2O)_2]\cdot H_2O\}_n$ (**a**)	10	2.598	–	–
$\{[Nd_2(L)_6(H_2O)]\cdot 4H_2O]\}_n$ (**b**)	10	2.546	9	2.496
$\{[Dy_2(L)_6(H_2O)]\cdot 3H_2O]\}_n$ (**d**)	8	2.374	9	2.432
$\{[Y_2(L)_6(H_2O)]\cdot 3H_2O]\}_n$ (**e**)	8	2.363	9	2.411
$\{[Er_2(L)_6(H_2O)]\cdot 5H_2O]\}_n$ (**f**)	9	2.409	8	2.347
$\{[Yb_2(L)_6(H_2O)]\cdot 5H_2O]\}_n$ (**g**)	9	2.403	8	2.326

considerably along the chain. The angles subtended at the three bridging oxygen atoms also are different with values of 102.613(6)° (Nd1-O2-Nd2), 98.662(7)° (Nd1-O5-Nd2), and 108.246(11)° (Nd1-O7-Nd2) in order.

The average Nd–O bond lengths for Nd1 and Nd2 with carboxylate oxygens (2.546 and 2.496 Å, respectively) (Table 2), are consistent with a change of one in coordination number.[44] The longer RE-O bonds, relieve steric strain at the metal center.[30]

Lattice water molecules through O11, and O12 form two H-bonds with the oxygen atoms of a hydroxyl group (O3) and carboxylate group (O1) respectively of the same ligand (Figure 5). H bond lengths of $\{[Nd_2(L)_6(H_2O)]\cdot 4H_2O\}_n$ are listed in Table S6, Supporting Information.

2.2.3. The Complexes $\{[RE_2(L)_6(H_2O)]\cdot 3H_2O]\}_n$ (RE = Dy, Y)

The polymeric complexes $\{[RE_2(L)_6(H_2O)]\cdot 3H_2O]\}_n$ (RE = Dy (**d**), Y (**e**)) have binuclear repeating units, and crystallize in the triclinic crystal system and the *P*1 space group (see SI for comment). As a representative, a section of the polymeric structure of $\{[Dy_2(L)_6(H_2O)]\cdot 3H_2O]\}_n$ are depicted in **Figure 6**. The asymmetric unit consists of two types of Dy^{III} ions, coordinated by six ligands and a water molecule, with three lattice water molecules (O20, O21, and O22).

The Dy1 ion has a coordination number of 8 with a bicapped trigonal prismatic array due to the coordination of six oxygen atoms (O1, O2, O7, O8, O4, and O10) of four chelating bridging ligands, two (O16, and O14#) from *syn-syn* bridging ligands. Of the chelating bridging ligands, two of them bind as bidentates to Dy1 (O1, O2; O7, O8) and the other two are monodentate (O4, O10). On the contrary, Dy2 is 9 coordinate resulting in a tricapped trigonal prismatic array. It has two chelating bridging carboxylates which chelate through O10, O11, O4*, O39*, two chelating bridging carboxylates binding through one oxygen atom of each (O8, and O1*), two *syn-syn* bridging carboxylate oxygen atoms (O13 and O17) and one water oxygen atom (O19). All Dy ions bind to their adjacent metal ion by chelating bridging carboxylates (O1, O4 or O8, O10) and syn-syn bridging (O13, O14 or O16, O17) forming a 1-D polymeric chain.

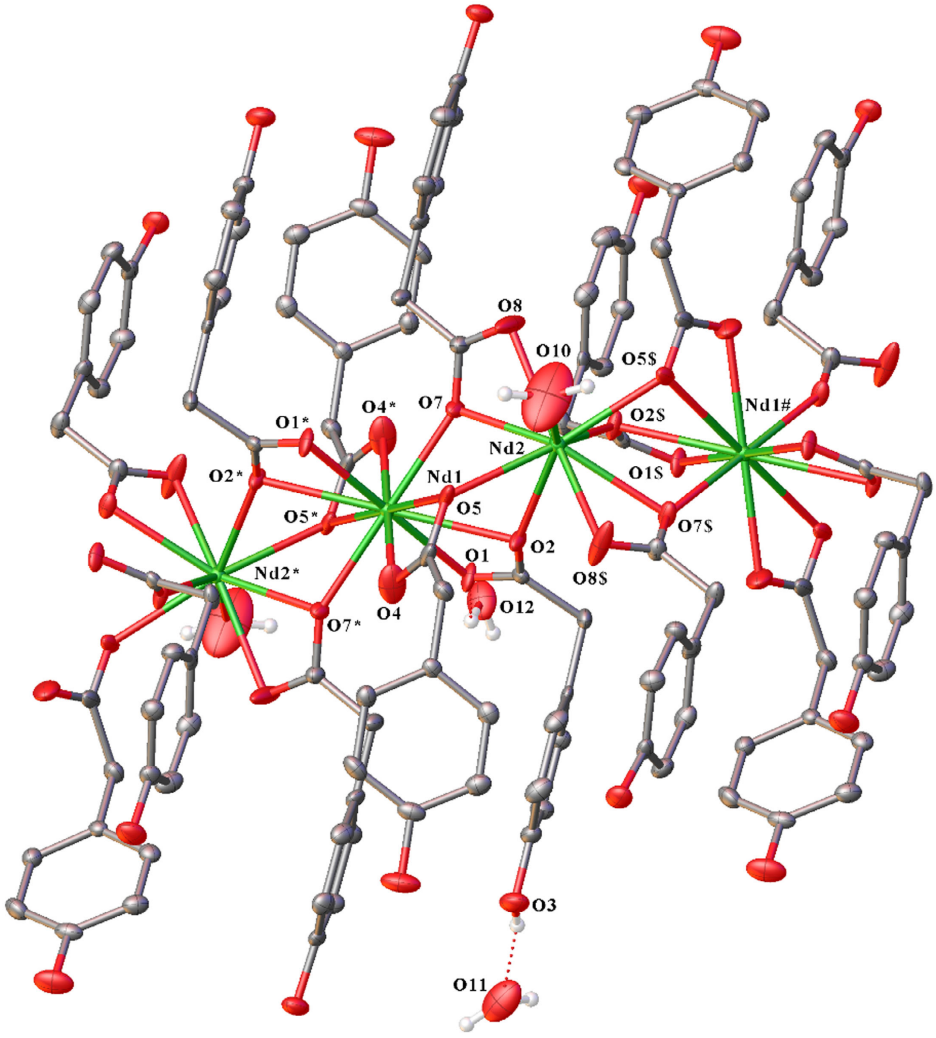

Figure 5. A part of the polymeric chain of $\{[Nd_2(L)_6(H_2O)]\cdot 4H_2O\}_n$ **b** (representative of complexes **b** and **c**) with 50% thermal ellipsoids. Hydrogen atoms have been omitted except of H-bond contributing atoms and coordinated water molecule for clarity. Symmetry Code: #(+X, 1 − Y, 1/2 + Z); *(1 − X, 1 − Y, 1 − Z); $(1 − X, +Y, 3/2 − Z).

The distance between adjacent metal centers is 4.039(3) Å (Dy1-Dy2), and 3.998(3) Å (Dy1-Dy2#). The angles Dy2-Dy1-Dy2#, and Dy1-Dy2-Dy1* are the same (168.371(11)°).

The shortest Dy–O bond lengths are subtended by bridging bidentate ligand O16, O17 to Dy1 and Dy2 respectively, their difference being slightly larger than expected for the difference in coordination number.[44] The longest Dy1–O bonds are Dy1-O7,O8 with near symmetrical chelation, whereas Dy2-O10 is 0.1 Å longer than any other bond of nine coordinate Dy2.

2.2.4. The Complexes $\{[RE_2(L)_6(H_2O)]\cdot 5H_2O]\}_n$ (RE = Er, Yb)

The complexes of Er (**f**) and Yb (**g**) with 4-hydroxyphenylacetate form a 1-dimensional, polymeric structure based on a dinuclear repeat unit. The complexes are isomorphous and crystallize in the monoclinic $P2_1$ space group. The representative structure of $\{[Er_2(L)_6(H_2O)]\cdot 5H_2O]\}_n$ is described. **Figure 7** presents a part of the polymer chain. The asymmetric unit of the Er complex consists of two different Er^{III} ions (Er1, and Er2), six ligands, one ligated water molecule, and five waters of crystallization.

Er1 ion is in a nine-coordination environment with a tricapped trigonal prismatic arrangement formed by six oxygen atoms from four chelating bridging ligand ions, two oxygens (O7, O16) from *syn-syn* bridging ligands and one oxygen (O19) from a water molecule. Out of four chelating bridging ligands, two are bidentate with Er1 sharing four oxygens (O1, O2, O10, O11), while the other two bind to Er1 by one oxygen from each (O4, O13). Eight coordinate Er2 has a bicapped trigonal prismatic coordination environment, and is bound by four chelating bridging tridentate carboxylates, (two ligands through four oxygen atoms (O4*, O5*, O13, O14), and other two ligands through two oxygens O1*, and O11), Two bridging bidentate carboxylates bind through two oxygens (O8* and O17).

To create this polymeric chain, the two neighboring metal centers are connected by two chelating bridging carboxylates (O1, O4 or O11, O13) ligands and one *syn-syn* bridging carboxylate (O7, O8 or O16, O17). The distance between the adjacent

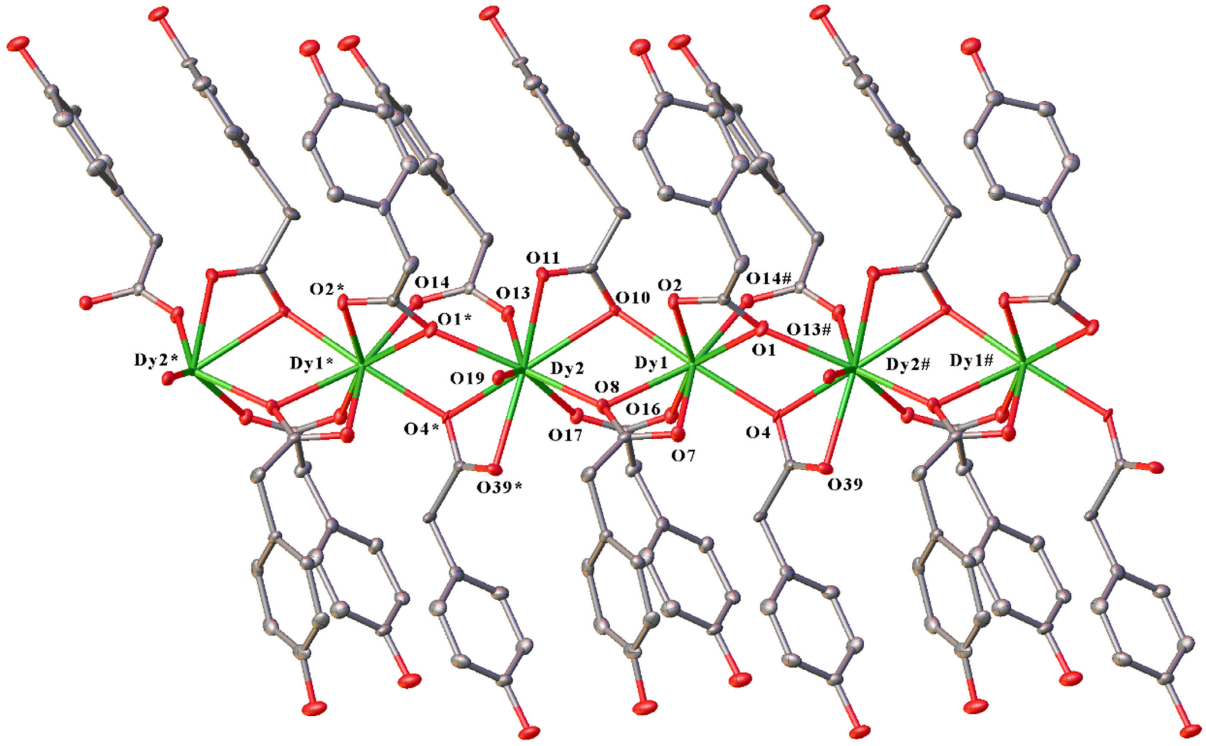

Figure 6. A part of the polymeric chain of $\{[Dy_2(L)_6(H_2O)]\cdot 3H_2O]\}_n$ **d** (represented of complexes **d** and **e**) with 50% thermal ellipsoids. Hydrogen atoms have been omitted for clarity. Symmetry Code: # −1 + X, 1 + Y, +Z; *1 + X, +Y, +Z.

metal centers is 3.97498(15) Å (Er1-Er2), and, 4.01001(15) Å (Er1-Er2#) with a similar angle of 167.5746(7)° at both types of metal ions (Er2-Er1-Er2# and Er1-Er2-Er1).

The average RE-O(carboxylate) bond lengths of nine-coordinated Er/Yb1 and eight-coordinated Er/Yb2 (Table 2) differ by more than expected[44] possibly owing to relief of steric strain at the lower coordinate ion. Average RE-O bond lengths of nine and eight coordinated spheres reduce within the series Nd2-O > Dy2-O > Y2-O > Er1-O > Yb1-O and Dy1-O > Y1-O > Er2-O > Yb2-O respectively (Table 2) as expected for the lanthanoid contraction.[44]

The five uncoordinated water molecules form H bonds with hydroxyl oxygens and carboxylic oxygens of the ligand as represented in Figure 7. Table S11, Supporting Information lists the experimental values of H bond lengths of both $\{[Er_2(L)_6(H_2O)]\cdot 5H_2O]\}_n$ and $\{[Yb_2(L)_6(H_2O)]\cdot 5H_2O]\}_n$.

2.3. Corrosion Inhibition

2.3.1. Weight Loss Testing

Weight loss tests were carried out to determine the percentage corrosion inhibition efficiency (IE%) of each synthesized RE complex. These tests were performed with 500 ppm of compound in 0.01 M NaCl aqueous solution at 25 °C for 168 h on AS1020 mild steel coupons (around 9 cm^2 of coupon area). The results are summarized in **Table 3**. At the end of the 7 day period, different degrees of corrosion were observed on tested coupons as presented in Figure S5, Supporting Information. Among all the compounds studied here, $[Ce(L)_3(H_2O)_2]\cdot H_2O$ exhibits the lowest corrosion inhibition, as well as the highest degree of corrosion products on the metal surface. The minimum corroded areas on the coupon surfaces were noted for the $[Gd_2(L)_6(H_2O)]\cdot 4H_2O$ complex and aligned with the highest % inhibition.

The corrosion inhibition performances of unsubstituted RE phenylacetate complexes with two different co-ligands (water and 2,2′-bipyridine (bpy)) on mild steel (2 cm^2 of coupon area) were previously reported (Table 3).[33] Compounds of both series were tested under comparable conditions. Under the low concentrations used, it is likely that all complexes breakdown to monomers, as a lanthanoid anthranilate and several lanthanoid salicylate inhibitors can be crystallized with monomeric structures from water.[45,46] It can be seen that the anti-corrosion properties of all RE complexes of 4-hydroxyphenylacetate outperformed the unsubstituted phenylacetate compounds (both aqua and bipyridine complexes). These observations indicate that introducing the 4-hydroxy group into the phenyl ring has led to marked enhancement of the inhibitor performance. Plausibly, the 4-OH substituent can undergo condensation with a surface FeOH group formed by corrosion thereby anchoring the inhibitor on the surface (Equation (2)), and thereby reducing the corrosion rate by forming a protective layer on the metal substrate.

$$-FeOH + HOC_6H_4CH_2CO_2RE- \rightarrow -FeOC_6H_4CO_2RE - + H_2O \quad (2)$$

Complex stability increases with the Ln contraction but this is not reflected in the inhibition efficiency order.

Journal of Inorganic and General Chemistry
ZAAC
Zeitschrift für anorganische und allgemeine Chemie

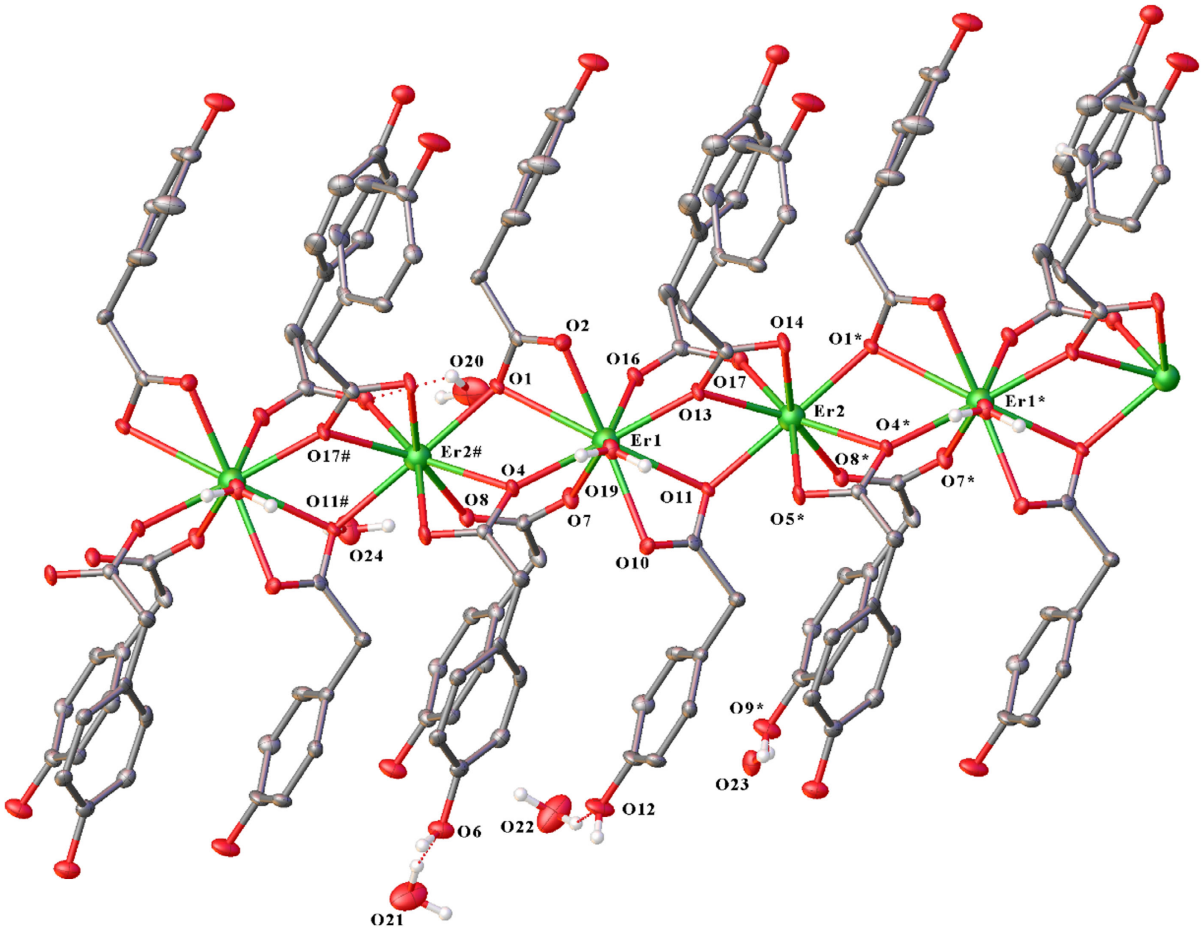

Figure 7. A part of the polymeric chain of $\{[Er_2(L)_6(H_2O)]\cdot 5H_2O]\}_n$ **e** (represented of complexes **e** and **f**) with 50% thermal ellipsoids. Hydrogen atoms have been omitted except of H-bond contributed atoms and coordinated water molecules for clarity. Symmetry Code: # −1 + X, +Y, +Z; *1 + X, +Y, +Z.

Table 3. Observed weight loss percentage, corrosion rates (mm year^{-1}) and percentage inhibition efficiency (IE%) of compounds a–g for mild steel coupons in inhibitor solutions of 500 ppm in 0.01M NaCl after 7 days of immersion.[33]

Solution	Concentration [ppm]	Concentration [mM]	Average weight loss percentage [%]	Corrosion rate [mm year^{-1}]	IE%
Control	580	10	0.36	0.135	–
$\{[La(PhAc)_3(H_2O)_2]_2\cdot 1/2\ bpy\}_n$	500	0.781	–	–	41
$\{[CeL)_3(H_2O)_2]\cdot H_2O\}_n$ (**a**)	500	0.772	0.11	0.043	68
$\{[Nd_2(L)_6(H_2O)]\cdot 4H_2O\}_n$ (**b**)	500	0.389	0.08	0.031	77
$[Nd(PhAc)_3(H_2O)]_n$	500	0.881	–	–	55
$[Nd(PhAc)_3bpy]_2$	500	0.354	–	–	46
$\{[Gd_2(L)_6(H_2O)]\cdot 4H_2O\}_n$ (**c**)	500	0.381	0.04	0.016	88
$[Gd(PhAc)_3(H_2O)]_n$	500	0.861	–	–	45
$\{[Dy_2(L)_6(H_2O)]\cdot 3H_2O\}_n$ (**d**)	500	0.383	0.1	0.036	73
$\{[Y_2(L)_6(H_2O)]\cdot 3H_2O\}_n$ (**e**)	500	0.432	0.08	0.030	78
$\{[Er_2(L)_6(H_2O)]\cdot 5H_2O\}_n$ (**f**)	500	0.371	0.1	0.037	73
$\{[Yb_2(L)_6(H_2O)]\cdot 5H_2O\}_n$ (**g**)	500	0.367	0.1	0.040	70

2.3.2. Potentiodynamic Polarization Measurements

Representative potentiodynamic polarization (PP) scans on mild steel in the absence and presence of inhibitor compound at 500 ppm are shown in Figure S6, Supporting Information. The results of the PP experiments, namely, corrosion current density (I_{corr}), corrosion potential (E_{corr}), and percentage inhibition efficiency (IE%) are given in **Table 4**. Significant reduction of the I_{corr} obtains when the inhibitor compounds are in the solution. Compound **c**, $\{[Gd_2(L)_6(H_2O)]\cdot 4H_2O\}_n$ showed the best, though

Table 4. Polarization parameters for mild steel in control and inhibited solutions after 24 h immersion.

Solution	I_{corr} [μA cm^{-2}]	E_{corr} [mV]	IE%
Control	3.93	−626	–
$\{[CeL)_3(H_2O)_2]\cdot H_2O\}_n$ (**a**)	1.03	−416	74
$\{[Gd_2(L)_6(H_2O)]\cdot 4H_2O\}_n$ (**c**)	0.83	−433	79
$\{[Y_2(L)_6(H_2O)]\cdot 3H_2O\}_n$ (**e**)	0.90	−429	77

only marginally, inhibition efficiency, 79% with the lowest I_{corr}, at 0.83 μA cm^{-2}. The E_{corr} values of all the inhibitor-solutions shift toward the positive direction, compared with the control, indicative of anodic inhibition behavior of the tested compounds.

3. Conclusions

A series of RE complexes with 4-hydroxyphenylacetate and aqua co-ligand was successfully synthesized and characterized. Four different crystal structures were obtained for the compounds, which are one-dimensional polymers. Except for the Ce complex, all other structures are based on binuclear repeating units. The chelating bridging coordination mode of the carboxylic group is common for all compounds, but the complexes of Dy, Y, Er, and Yb have additional *syn-syn* bridging, while *syn-syn* chelation is observed in the Ce complex. The decline in the average RE-O (carboxylate) bond distance for the same coordination number, across the lanthanide series is as expected for the lanthanoid contraction. In corrosion tests conducted on mild steel using the weight loss method, $\{[Gd_2(L)_6(H_2O)]\cdot 4H_2O]\}_n$ exhibited the highest inhibition efficiency (88%). Corrosion inhibition efficiency results from potentiodynamic polarization also confirm the effectiveness of compound **c** giving marginally the highest percentage inhibition. All compounds in this study are more efficient than the RE unsubstituted phenylacetates,[33] illustrating the value of introducing the 4-hydroxy substituent.

4. Experimental Section

General Considerations: All standard commercial grade reagents and solvents were used without further purification. FTIR data were obtained in the region 4000–500 cm^{-1} by using a Nicolet iS 5 FTIR Spectrometer. Elemental analyses (C, H) were effected by the Microanalytical Laboratory at the Science Center, London Metropolitan University, England. Metal percentages of the complexes were found through complexometric titration with 0.01 M EDTA, using Xylenol Orange as the indicator and hexamethylenetetramine buffer.[47–49] The aqueous metal solution used for metal analysis was prepared by dissolving the compound in distilled water with the addition of some dilute HCl. Thermogravimetric analysis (TGA) was carried out using a TA instrument SDT 650 with standard 90 μL alumina metal pans under a N_2 atmosphere at a flow rate of 50 mL min^{-1}. The temperature range was from room temperature to 750 °C with a ramp of 10 °C min^{-1}. Melting points were determined using glass capillary tubes and are reported without calibration. Powder X-ray diffractograms were obtained at room temperature using a Bruker D2 PHASER diffractometer in the range of 5°–50° of 2θ with a 0.2° divergence slit and at 0.02° increments. X-ray powder simulations were generated by the Mercury program provided by the Cambridge Crystallographic Data Center, based on the experimental single-crystal X-ray diffraction data. Crystals were measured on a Bruker D8 Quest. Crystal data and refinement details are given in Table S1, Supporting Information. CCDC **2385814–2385815** for compounds **a–b**, **2385816–2385819** for compounds **d–g**, contain the supplementary crystallographic data for this article. These data can be obtained free of charge from The Cambridge Crystallographic Data Center via www.ccdc.cam.ac.UK/data_request/cif.

Synthesis of 4-Hydroxyphenylacetate (L) RE Complexes: General Synthetic Method: 4-Hydroxyphenyl acetic acid (1.5 mmol) was dissolved in 95% ethanol (1 mL) and 3 mL of distilled water, and then reacted with an equimolar amount of sodium hydroxide (1.5 mmol) in 6 mL of distilled water. Then the pH of the solution was adjusted within the range 7–8. Subsequently, an aqueous RE chloride or nitrate solution (0.5 mmol) was slowly treated with three molar equivalents of prepared sodium 4-hydroxyphenyl acetate and stirred for 2 h at pH 6. The resultant colloidal solution was filtered. The filtrate was allowed to slowly evaporate and grow crystals. The crystals and any precipitate were air dried for 2 days.

a:$\{[Ce(L)_3(H_2O)_2]\cdot H_2O\}_n$ Yield: 0.263 g, 81%. m.p. 230 °C (dec). Elemental analysis for $C_{24}H_{27}CeO_{12}$ (MW: 647.57 gmol^{-1}): Calculated (%) C 44.51, H 4.20, Ce 21.64; Found (%) C 44.43, H 3.94, Ce 21.75. IR (cm^{-1}): 3281 br w, 1598, 1576 w, 1546 m, 1513 s, 1432 m, 1403 s, 1388, 1298 w, 1245 s, 1221, 1202, 1168 m, 1098, 949, 938, 925, 862, 821 w, 795, 736 m, 694 s, 646 w, 594, 555 m, 539, 508 s. TGA weight loss (25–150 °C); 8.2% (1st step - 5.6%, 2nd step - 2.6%) (Calc. for loss of 3 × H_2O = 8.3%).

b:$\{[Nd_2(L)_6(H_2O)]\cdot 4H_2O\}_n$ Yield: 0.272 g, 85%. m.p. 273 °C (dec). Elemental analysis for $C_{48}H_{52}Nd_2O_{23}$ (MW: 1285.39 gmol^{-1}): Calculated (%) C 44.85, H 4.08, Nd 22.44; Found (%) C 44.81, H 3.58, Nd 22.56. IR (cm^{-1}): 3271 br w, 1599 m, 1571 w, 1542 m, 1515, 1442, 1419, 1397 s, 1282 m, 1247 s, 1205 w, 1175, 1155, 1098 m, 1018, 950, 929, 862, 829 w, 807, 792 m, 737, 694 s, 650, 633, 591, 551 m, 510 s. TGA weight loss (25–150 °C); 6.9% (Calc. for loss of 5 × H_2O = 7.0%).

c:$\{[Gd_2(L)_6(H_2O)]\cdot 4H_2O\}_n$ Yield: 0.235 g, 72%. m.p. 267 °C (dec). Elemental analysis for $C_{48}H_{52}Gd_2O_{23}$ (MW: 1311.41 gmol^{-1}): Calculated (%) C 43.96, H 4.00, Gd 23.98; Found (%) C 43.85, H 3.50, Gd 23.57. IR (cm^{-1}): 3304 br w, 1599, 1576 w, 1542 m, 1516 s, 1445 m, 1421, 1401 s, 1283 m, 1247 s, 1206 w, 1176, 1157, 1098 m, 1018, 955, 930, 861, 829 w, 808, 791, 740, 696 s, 651, 634, 592, 553 m, 509 s. TGA weight loss (25–150 °C); 7.5% (Calc. for loss of 5 × H_2O = 6.9%).

d:$\{[Dy_2(L)_6\cdot H_2O]\cdot 3H_2O\}_n$ Yield: 0.214 g, 66%. m.p. 268 °C (dec). Elemental analysis for $C_{48}H_{50}Dy_2O_{22}$ (MW: 1303.90 gmol^{-1}): Calculated (%) C 44.21, H 3.86, Dy 24.93; Found (%) C 44.20, H 3.40, Dy 24.77. IR (cm^{-1}): 3569 w, 3333 br w, 1603 w, 1530, 1514, 1405 s, 1283 m, 1240 s, 1172, 1099 m, 1021, 951, 861 w, 823, 797, 738, 727, 695, 644 m, 609, 538, 508 s. TGA weight loss (25–150 °C); 5.8% (Calc. for loss of 4 × H_2O = 5.5%).

e:$\{[Y_2(L)_6\cdot H_2O]\cdot 3H_2O\}_n$ Yield: 0.201 g, 70%. m.p. 267 °C (dec). Elemental analysis for $C_{48}H_{50}O_{22}Y_2$ (MW: 1156.71 gmol^{-1}): Calculated (%) C 49.84, H 4.36, Dy 15.37; Found (%) C 50.12, H 4.11, Y 15.22. IR (cm^{-1}): 3568 w, 3276 br w, 1601, 1579 w, 1530, 1514, 1405 s, 1284 m, 1241 s, 1170, 1099 m, 1020, 951, 864 w, 823, 797, 738, 729, 695, 646, 605 m, 537, 507 s. TGA weight loss (25–150 °C); 7.0% (Calc. for loss of 4 × H_2O = 6.2%).

f:$\{[Er_2(L)_6\cdot H_2O]\cdot 5H_2O\}_n$ Yield: 0.175 g, 52%. m.p. 268 °C (dec). Elemental analysis for $C_{48}H_{54}Er_2O_{24}$ (MW: 1349.44 gmol^{-1}): Calculated (%) C 42.72, H 4.03, Er 24.79; $C_{48}H_{50}Er_2O_{22}$ (MW: 1313.41 gmol^{-1}, loss of 2 H_2O of crystallization): C 43.89, H 3.84, Er 25.47; Found (%) C 44.13, H 3.38, Er 25.68. IR (cm^{-1}): 3569 w, 3327 br w, 1599 w, 1528, 1514, 1405 s, 1284 m, 1240 s, 1171, 1099 m, 1020, 952, 861 w, 823, 797, 739, 727, 695, 644, 610 m, 536, 507 s. TGA weight loss (25–150 °C) for $C_{48}H_{50}Er_2O_{22}$ (loss of 2 H_2O of crystallization, $\{[Er_2(L)_6\cdot H_2O]\cdot 3H_2O\}_n$): 5.7% (Calc. for loss of 4 × H_2O = 5.5%).

g:{$[Yb_2(L)_6{\cdot}H_2O]{\cdot}5H_2O\}_n$, Yield: 0.196 g, 58%. m.p. 268 °C (dec). Elemental analysis for $C_{48}H_{54}O_{24}Yb_2$ (MW: 1361.01 $gmol^{-1}$): Calculated (%) C 2.36, H 4.00, Yb 25.43; Found (%) C 42.35, H 3.54, Yb 25.15. IR (cm^{-1}): 3569 w, 3327 br w, 1600 w, 1534, 1514, 1400 s, 1284 m, 1241 s, 1171, 1100 m, 1020, 957 w, 825, 798, 744, 728, 697, 645, 612 m, 507 s. TGA weight loss (25–150 °C); 8.2% (Calc. for loss of $6 \times H_2O = 7.9\%$).

Corrosion Testing: Weight loss measurements were carried out following the standard methods ASTM G31-72,[50] and G1-03[51] to estimate the corrosion inhibition properties of the synthesized compounds. Mild-steel alloy AS 1020 coupons with dimensions of ≈20 × 20 × 2 mm were used as test specimens for the current study. The corrosion rates (*R*) of the inhibitor solutions and the control were calculated using the Equation (3) and the average of measurements were reported.

$$\text{Corrosion Rate}\,(R) = (K \times W)/A \times T \times D \quad (3)$$

where *K* is a constant (*K* = 87 600); *W* is the weight loss in grams; *A* is the coupon area (cm^2); *T* is the time of exposure (168 h); *D* is the density of the coupon material (7.87 g cm^{-3}).

Then the percentage corrosion inhibition efficiency (IE%) of each compound solution at given concentration, was determined comparable to the control test using Equation (4).

$$\text{IE\%} = [R(\text{control}) - R(\text{inhibitor})/R(\text{control})] \times 100 \quad (4)$$

The potentiodynamic polarization (PP) experiments were performed using a BioLogic VMP3 potentiostat controlled with EC Lab V10.57 software. The experimental setup was open-to-air three-electrode cell consists of mild steel as the working electrode (WE) with a surface area of 0.785 cm^2, a titanium mesh counter electrode (CE), and a saturated Ag/AgCl reference electrode (RE). After immersing the electrodes in 150 mL of test solution, the set-up was allowed to rest at open circuit voltage (OCV) for 24 h. The PP scan was carried out with a scan rate of 0.167 mV s^{-1} within the range of 150 mV, below OCV (60 mV for the control solution) and 250 mV, more positive than OCV. The corrosion potential (E_{corr}) and corrosion current density (I_{corr}) were determined via Tafel extrapolation. E_{corr} was first assessed by inspection, and linear fits were made over the 20–40 mV range on either side of the E_{corr} to get the Tafel slopes converge at the observed E_{corr}. The PP tests were repeated for each condition.

The percentage inhibitor efficiency (IE%) was calculated using the Equation (5) below:

$$\text{IE\%} = [(I_{corr}(\text{control}) - I_{corr}(\text{inhibitor})/I_{corr}(\text{control})] \times 100 \quad (5)$$

Acknowledgements

P.C.J. and G.B.D. gratefully acknowledge the ARC for funding (DP200100568). P.C.J. and Z.G. acknowledge James Cook University for internal funding.

Conflict of Interest

The authors declare no conflict of interest.

Data Availability Statement

The data that support the findings of this study are available from the corresponding author upon reasonable request.

Keywords: carboxylates · corrosion inhibitors · crystal structures · 4-hydroxyphenylacetate · mild steel · rare-earth metals

[1] A. Kadhim, A. A. Al-Amiery, R. Alazawi, M. K. S. Al-Ghezi, R. H. Abass, *Int. J. Corros. Scale Inhib.* **2021**, *10*, 54.
[2] A. A. Olajire, *J. Mol. Liq.* **2017**, *248*, 775.
[3] M. Forsyth, M. Seter, B. Hinton, G. Deacon, P. Junk, *Aust. J. Chem.* **2011**, *64*, 812.
[4] A. Kadhim, N. Betti, H. A. Al-Bahrani, M. K. S. Al-Ghezi, T. Gaaz, A. H. Kadhum, A. Alamiery, *Int. J. Corros. Scale Inhib.* **2021**, *10*, 861.
[5] M. H. Bui, S. H. Hiew, T. Salim, W. G. Saw, R. D. Webster, G. Grüber, Y. Mu, A. Miserez, *Commun. Mater.* **2024**, *5*, 11.
[6] W. R. de Souza Morais, J. S. da Silva, N. M. P. Queiroz, C. L. de Paiva e Silva Zanta, A. S. Ribeiro, J. Tonholo, *Appl. Sci.* **2023**, *13*, 7482.
[7] Y. H. A. Akbari, M. Rostami, M. G. Sari, B. Ramezanzadeh, *J. Mol. Struct.* **2024**, *1309*, 138034.
[8] C. Machado Fernandes, M. S. Coutinho, M. C. Leite, V. Martins, M. P. Batista, L. V. Faro, A. A. Al-Rashdi, J. C. M. Silva, P. N. Batalha, H. Lgaz, E. A. Ponzio, *Inorg. Chem. Commun.* **2024**, *159*, 111722.
[9] M. A. Quraishi, D. S. Chauhan, V. S. Saji, *Heterocyclic Organic Corrosion Inhibitors: Principles and Applications*, Elsevier, Amsterdam **2020**.
[10] M. Forsyth, M. Seter, M. Y. Tan, B. Hinton, *Corros. Eng. Sci.* **2014**, *49*, 130.
[11] Y. Peng, A. E. Hughes, G. B. Deacon, P. C. Junk, B. R. W. Hinton, M. Forsyth, J. I. Mardel, A. E. Somers, *Corros. Sci.* **2018**, *145*, 199.
[12] O. Sanumi, E. Makhatha, in *2018 IEEE 9th Int. Conf. Mechanical and Intelligent Manufacturing Technologies (ICMIMT)*, Cape Town, South Africa **2018**, pp. 69–73.
[13] J. Sinko, *Prog. Org. Coat.* **2001**, *42*, 267.
[14] J. De Damborenea, A. Conde, M. A. Arenas, *Rare Earth-Based Corrosion Inhibitors* (Eds: M. Forsyth, B. Hinton), Woodhead Publishing Limited, Cambridge **2014**, pp. 84–116.
[15] B. R. W. Hinton, *Met. Forum* **1984**, *7*, 221.
[16] B. R. W. Hinton, D. R. Arnott, N. E. Ryan, *Mater. Forum* **1986**, *9*, 162.
[17] K. Tamalmani, H. Husin, *Appl. Sci.* **2020**, *10*, 3389.
[18] W. Li, Q. He, C. Pei, B. Hou, *Electrochim. Acta* **2007**, *52*, 6386.
[19] J. Saranya, M. Sowmiya, P. Sounthari, K. Parameswari, S. Chitra, K. Senthilkumar, *J. Mol. Liq.* **2016**, *216*, 42.
[20] C. Verma, E. E. Ebenso, M. A. Quraishi, *J. Mol. Liq.* **2017**, *248*, 927.
[21] M. Goyal, S. Kumar, I. Bahadur, C. Verma, E. E. Ebenso, *J. Mol. Liq.* **2018**, *256*, 565.
[22] C. Verma, E. E. Ebenso, M. A. Quraishi, C. M. Hussain, *Mater. Adv.* **2021**, *2*, 3806.
[23] M. Forsyth, C. M. Forsyth, K. Wilson, T. Behrsing, G. B. Deacon, *Corros. Sci.* **2002**, *44*, 2651.
[24] M. Forsyth, K. Wilson, T. Behrsing, C. Forsyth, G. B. Deacon, A. Phanasgoankar, *Corrosion* **2002**, *58*, 953.
[25] F. Blin, S. G. Leary, K. Wilson, G. B. Deacon, P. C. Junk, M. Forsyth, *J. Appl. Electrochem.* **2004**, *34*, 591.
[26] F. Blin, S. G. Leary, G. B. Deacon, P. C. Junk, M. Forsyth, *Corros. Sci.* **2006**, *48*, 404.
[27] A. E. Somers, Y. Peng, A. L. Chong, M. Forsyth, D. R. MacFarlane, G. B. Deacon, A. E. Hughes, B. R. W. Hinton, J. I. Mardel, P. C. Junk, *Corros. Eng., Sci. Technol.* **2020**, *55*, 311.
[28] G. B. Deacon, P. C. Junk, W. W. Lee, M. Forsyth, J. Wang, *New J. Chem.* **2015**, *39*, 7688.
[29] V. P. Vithana, Z. Guo, G. B. Deacon, A. E. Somers, P. C. Junk, *New J. Chem.* **2022**, *46*, 19104.

[30] V. P. Vithana, Z. Guo, G. B. Deacon, P. C. Junk, *Eur. J. Inorg. Chem.* **2024**, *27*, e202300722.
[31] J. Moon, Z. Guo, O. A. Beaumont, S. Hamilton, G. Bousrez, E. Mottram, J. Wang, A. E. Somers, G. B. Deacon, P. C. Junk, *New J. Chem.* **2023**, *47*, 16843.
[32] V. P. Vithana, Z. Guo, G. B. Deacon, A. E. Somers, P. C. Junk, *Molecules* **2022**, *27*, 8836.
[33] E. Mottram, S. Hamilton, J. S. Moon, J. Wang, G. Bousrez, A. E. Somers, G. B. Deacon, P. C. Junk, *J. Coord. Chem.* **2020**, *73*, 2677.
[34] R. Janicki, A. Mondry, P. Starynowicz, *Coord. Chem. Rev.* **2017**, *340*, 98.
[35] F. E. Öztürkkan, E. Teymouri, M. Yüksek, E. Akhüseyin Yıldız, M. Sertçelik, A. Alemi, H. Necefoğlu, T. Hökelek, *Mater. Sci. Eng., B* **2023**, *290*, 116331.
[36] S. Y. Yang, Q. Zhang, Y. L. Zhang, T. S. Tan, J. Zhu, X. Yang, L. Shi, J. Yang, D. Shao, *CrystEngComm* **2024**, *26*, 4181.
[37] D. Q. Wu, Z. Fan, Q. Zhang, L. Y. Yi, Q. Gu, J. Dong, L. Huang, J. Yang, D. Shao, B. Zhai, *J. Mol. Struct.* **2024**, *1306*, 137874.
[38] Q. Zhang, S. Y. Yang, S. J. Chen, L. Shi, J. Yang, Z. Tian, Z. Ruan, D. Shao, *J. Mol. Struct.* **2023**, *1294*, 136349.
[39] D. Shao, Y. Wan, J. Yang, Z. Ruan, J. Zhu, L. Shi, *Dalton Trans.* **2023**, *52*, 17114.
[40] H. Zhang, G. Y. Liu, X. H. Diao, Y. Muhammad, C. Chen, Y. Y. Gao, H. Wang, C. S. Qi, W. Li, *J. Solid State Chem.* **2023**, *324*, 124114.
[41] A. Aragón-Muriel, M. Camprubí-Robles, E. González-Rey, A. Salinas-Castillo, A. Rodríguez-Diéguez, S. Gómez-Ruiz, D. Polo-Cerón, *Polyhedron* **2014**, *80*, 117.
[42] K. Nakamoto, *Infrared and Raman Spectra of Inorganic and Coordination Compounds, Part B: Applications in Coordination, Organometallic, and Bioinorganic Chemistry*, John Wiley & Sons, New Jersey **2009**.
[43] G. B. Deacon, R. J. Phillips, *Coord. Chem. Rev.* **1980**, *33*, 227.
[44] R. D. Shannon, *Acta Crystallogr.* **1976**, *A32*, 751.
[45] T. Behrsing, G. B. Deacon, J. Luu, P. C. Junk, B. W. Skelton, A. H. White, *Polyhedron* **2016**, *120*, 69.
[46] G. B. Deacon, M. Forsyth, P. C. Junk, S. G. Leary, G. J. Moxey, *Polyhedron* **2006**, *25*, 379.
[47] G. Schwarzenbach, H. Flascha, *Complexometric Titrations*, Methuen and Co. Ltd., London **1969**.
[48] T. S. West, *Complexometry with EDTA and Related Agents*, BDH Chemical Ltd., Poole, England **1969**, p. 46.
[49] W. Wagner, C. Hull, *Treatise on Titrimetry*, Dekker, New York **1971**.
[50] ASTM G31-72, ASTM International **2004**.
[51] ASTM G1-03, ASTM International **2017**.

Manuscript received: October 7, 2024
Revised manuscript received: November 12, 2024
Version of record online: January 22, 2025